Energy-resolved electron momentum densities of diamond-structure semiconductors

1995 J. Phys.: Condens. Matter 7 1821

(http://iopscience.iop.org/0953-8984/7/9/008)

J. Phys.: Condens. Matter 7 (1995) 1821–1833. Printed in the UK

Energy-resolved electron momentum densities of diamond-structure semiconductors

A S Kheifets† and Y Q Cai

Electronic Structure of Materials Centre, The Flinders University of South Australia, GPO Box 2100, Adelaide 5001, Australia

Received 8 November 1994

Abstract. The linear muffin-tin orbital (LMTO) method has been used to calculate energy and momentum distributions of valence electrons in diamond, silicon, germanium and grey tin along [100], [110] and [111] directions and as the spherical average over the irreducible wedge of the Brillouin zone. These data can be used for interpreting results of (e, 2e) experiments on single-crystal, polycrystalline and amorphous targets.

1. Introduction

Since the introduction of the density functional theory (DFT) (Hohenberg and Kohn 1964) and the local density approximation (LDA) (Kohn and Sham 1965) some thirty years ago, enormous progress has been achieved in the field of first-principles theoretical calculations of the ground-state properties of bulk semiconductors, their surfaces and interfaces (Lundqvist and March 1983, Bassani *et al* 1985). The density functional theory in principle provides an exact formalism for the ground-state energy. The local density approximation reduces the many-body problem to the self-consistent solution of a set of effective one-particle equations. On this basis, many calculation methods have been developed which have the computational efficiency and accuracy for a wide range of materials. For the valence band structure of bulk semiconductors, in particular, the difference between the results of different computational schemes is often less than the best experimental resolution available nowadays from techniques such as angle-resolved photoemission (Leckey and Riley 1992). The biggest drawback of the local density approximation is that the one-particle eigenvalues can not be interpreted formally as quasiparticle energies. When compared to optical data, band gaps in semiconductors are typically underestimated by 30–50%, and in particular cases like Ge the gap is closed when relativistic effects are taken into consideration (Bachelet and Christensen 1985). To account for this discrepancy, the latest development in this area has been the use of the so-called GW approximation (GWA) for the evaluation of the electron self-energy operator and has led to excellent agreement with a large body of experimental data (Hybertsen and Louie 1986a, Rohlfing *et al* 1993a), including in particular those concerning the conduction bands obtained from inverse photoemission (Ortega and Himpsel 1993). Nevertheless, these quasiparticle calculations produced essentially the same results as those produced by calculations based on the local density approximation as far as the relative energies of the valence bands are concerned (see further discussion in section 4), the improvement having been mainly on the prediction of the conduction bands and of the band gaps.

† email address: anatoli@esm.ph.flinders.edu.au.

0953-8984/95/091821+13$19.50

On the other hand, theoretical valence-band-structure calculations in the past have been tested almost exclusively in terms of energy, i.e., the eigenvalues of the Kohn–Sham equations (Kohn and Sham 1965). In contrast, relatively little attention has been directed towards the wave-function (i.e., the eigenfunction) of the electrons. This is despite the fact that wave function information provides a more sensitive way of testing the computational scheme under investigation if the electron wave function can be measured experimentally. Direct measurements of the wave function are not available at the present time, but it is known that under the independent-particle approximation the spectral momentum density (SMD) $\rho(\epsilon, q)$ is proportional to the square of the one-electron wave function in the momentum space. Since $\rho(\epsilon, q)\, d\epsilon\, dq$ gives the probability of finding an electron within the energy and momentum ranges of ϵ to $\epsilon + d\epsilon$ and q to $q + dq$, respectively, the SMD dictates the electronic properties of solids. Partial information on the momentum density can be obtained readily from Compton profiles (Cooper 1985) and from the angular correlation of positron annihilation radiation (Jain *et al* 1985). In terms of a full testing of the wave function, the energy-resolved electron momentum spectroscopy (EMS) based on the (e, 2e) reaction (McCarthy and Weigold 1988, 1991) provides enormous potential. The EMS has achieved great success in the study of the momentum distribution of valence electrons in gas targets (McCarthy and Weigold 1988, 1991). For solid materials, a series of recent experiments have also been successfully performed on various amorphous and disordered thin-film targets (Vos *et al* 1994, 1995b, a, Cai *et al* 1995b, a, Storer *et al* 1995), calling for theoretical studies of the spectral momentum density. For this purpose, it is appropriate to revisit existing computational techniques. This would not only provide a more sensitive way of testing the calculation technique, but also provide the necessary theoretical data for interpreting experimental (e, 2e) results.

We have studied the SMD of diamond-structure semiconductors, including diamond (C), silicon (Si), germanium (Ge) and grey tin (α-Sn), using the linear muffin-tin orbital (LMTO) method. In the present paper, the results for the three major symmetry directions [001], [110] and [111] (i.e. along the symmetry axes Δ, Σ and Λ, respectively) and as the spherical average over the irreducible wedge of the face-centred cubic (FCC) Brillouin zone will be presented. As recent (e, 2e) studies of the SMD of evaporated amorphous diamond (Storer *et al* 1995), silicon (Vos *et al* 1995a), germanium (Cai *et al* 1995a) and polycrystalline silicon carbide (Cai *et al* 1995b) showed, the spherical averaging of the spectral momentum density can be used to study amorphous and disordered materials.

The rest of the paper will be organized as follows. In section 2 we outline the LMTO method and specify the atomic sphere parameters used in our calculation. In section 3 we express the SMD in terms of the LMTO eigenfunctions and link it with various forms of the differential cross-sections obtained from the (e, 2e) reaction. The band-structure calculation results are discussed in section 4.1 in comparison with other theoretical and experimental data available to date. Directional and spherically averaged SMD are presented in section 4.2. Finally the results are summarized in section 5.

2. The LMTO method

The formalism of the LMTO method has been described in details in the monograph of Skriver (1984). The essence of the method is that for the atomic polyhedra a number of atomic spheres are substituted, each of which represents a non-equivalent atomic position.

The total volume of the spheres is equated to the volume of the elementary cell:

$$\sum_s \frac{4}{3}\pi R_s^3 = \Omega \tag{1}$$

where R_s is the muffin-tin (MT) radius of a sphere at site s.

The electron potential is spherically symmetric within the spheres. The tails of the LMTO orbitals outside the spheres are chosen to have zero kinetic energy. The Bloch sum of the tails is cancelled within the spheres. So the one-electron wave function within any particular sphere centred at r_s can be written as

$$\psi_{jk}(r - r_s) = \sum_{lm} a_{slm}^{jk} i^l Y_{lm}(\hat{r}_1)\frac{1}{r_1}P_{sl}(r_1) \qquad r_1 = |r - r_s| \leqslant R_s. \tag{2}$$

Here k is the crystal wave vector, j is the band index, Y_{lm} is the spherical harmonic depending on the orbital momentum l and its projection m. The expansion coefficients a_{slm}^{jk} for a given MT sphere s are found by solving the LMTO eigenvalue problem. The radial part of the wave function $P_{sl}(r)$ depends on the type of atom at site s and the orbital momentum l but does not depend on k and j which increases significantly the computational efficiency of the LMTO method.

The diamond structure elementary cell has two non-equivalent atomic positions at $(0, 0, 0)$ and $(a/4, a/4, a/4)$ where a is the lattice parameter. This structure is, however, far from close packing with only 0.34 of the cell volume filled with touching spheres. We follow the treatment of the 'open' diamond structure by Glötzel *et al* (1980) who suggested inserting two empty atomic spheres at the interstitial sites. We choose these sites at $(-a/4, -a/4, -a/4)$ and $(a/2, 0, 0)$.

The MT radius corresponding to four equal-size spheres is calculated from (1) as

$$R_s = \frac{a}{4}\left(\frac{3}{\pi}\right)^{1/3} = 0.2462\,a. \tag{3}$$

We use the MT radii given in table 1 which we calculate with the lattice parameters obtained from the book of Cohen and Chelikowsky (1988). We chose the maximum orbital momentum $l_{\max} = 2$ in the LMTO expansion (2).

Table 1. Lattice parameters and MT radii (in atomic units).

	Lattice parameter		MT radius
Material	(Å)	(au)	(au)
Diamond	3.567	6.742	1.659
Silicon	5.431	10.263	2.527
Germanium	5.657	10.690	2.632
Grey tin	6.491	12.267	3.020

3. The spectral momentum density

By definition, the SMD is expressed through the Fourier transform of the one-electron wave function ψ_{jk}:

$$\rho_j(\epsilon, q) = (2\pi)^{-3}\sum_{Gk} n_{jk}\left|\int \mathrm{d}^3r\ \psi_{jk}(r)\mathrm{e}^{-\mathrm{i}q\cdot r}\right|^2 \delta_{q,k+G}\,\delta(\epsilon - E_j(k)) \qquad k \in 1\text{st BZ} \tag{4}$$

Here n_{jk} and E_{jk} are the occupation number and energy of the corresponding one-electron state. The integration in (4) is carried out over the unit cell where the wave function ψ_{jk} is normalized to unity. The reciprocal-lattice vector G translates the momentum q to the first Brillouin zone (BZ). The SMD is normalized over energy and momentum space to the number of valence electrons per unit cell per spin:

$$2\sum_j \int \mathrm{d}\epsilon\ \mathrm{d}q\ \rho_j(\epsilon, q) = N_e. \tag{5}$$

The SMD gives the probability of finding an electron in band j within the unit range of the energy and momentum space. This is the most detailed information about electron distribution in solids. Less specific distributions can be obtained by the partial integration of the SMD over momentum or energy which gives either the density of states:

$$2\sum_j \int \mathrm{d}q\ \rho_j(\epsilon, q) = N(\epsilon) \tag{6}$$

or the energy-integrated electron momentum density (EMD)

$$\int \mathrm{d}\epsilon\ \rho_j(\epsilon, q) = \rho_j(q) \tag{7}$$

where according to (4)

$$\rho_j(q) = (2\pi)^{-3} \sum_{Gk} n_{jk} \left| \int \mathrm{d}^3 r\ \psi_{jk}(r) \mathrm{e}^{-\mathrm{i}q\cdot r} \right|^2 \delta_{q,k+G}. \tag{8}$$

Taking advantage of the central-field expansion (2) the SMD can be readily calculated as

$$\rho_j(\epsilon, q) = \frac{2}{\pi} \sum_{Gk} n_{jk} \left| \sum_s \mathrm{e}^{-\mathrm{i}q\cdot r_s} \sum_{lm} a_{slm}^{jk} Y_{lm}(\hat{k}) \int_0^{R_s} \mathrm{d}r\ j_l(qr) P_{sl}(r) \right|^2 \delta_{q,k+G}\, \delta(\epsilon - E_j(k)) \tag{9}$$

where $j_l(qr)$ is the spherical Bessel function. The expansion coefficients a_{slm}^{jk} and the one-electron energies $E_j(k)$ are found solving the LMTO eigenvalue problem.

The SMD can be obtained experimentally from the energy-resolved electron momentum spectroscopy based on the (e, 2e) reaction. In this reaction a primary fast electron knocks out a bound electron from the solid and both secondary electrons are detected in time coincidence with fully determined kinematics. When the energy of the primary and two secondary electrons is large enough one can think of the (e, 2e) reaction as a free-electron–electron collision satisfying the energy and momentum conservation laws:

$$\epsilon + E_0 = E_a + E_b \qquad q + k_0 = k_a + k_b. \tag{10}$$

Here we supply indices 0, a and b to the primary and two secondary electrons, respectively. The binding energy ϵ and momentum q refer to the initially bound electron.

The cross-section of the (e, 2e) reaction gives the probability of finding the two secondary electrons within the unit range of energy and momentum space. Because of the energy and momentum conservation (10) this is equivalent to finding the bound electron within the unit interval of the binding energy $\mathrm{d}\epsilon$ and the momentum $\mathrm{d}q$. The latter probability is given by the SMD. So the (e, 2e) cross-section can be written as (Persiantseva *et al* 1991, Allen *et al* 1990)

$$\frac{\mathrm{d}\sigma_j}{\mathrm{d}\Omega_a\ \mathrm{d}\Omega_b\ \mathrm{d}E_a\ \mathrm{d}E_b} = (2\pi)^4 N\ \frac{k_a k_b}{k_0} \left(\frac{\mathrm{d}\sigma}{\mathrm{d}\Omega}\right)_{\mathrm{Mott}} \rho_j(\epsilon, q) \tag{11}$$

where the Mott cross-section describes free-electron–electron scattering in the laboratory frame and N is the number of unit cells in the crystal.

A partial energy integration can be performed in (11) using the definition of the SMD (4) and the energy conservation (10)

$$\int \mathrm{d}E_b\, \delta(E_a + E_b - E_0 - E_j(\boldsymbol{k})) = 1 + \nabla E_j(\boldsymbol{k}) \cdot \boldsymbol{k}_b / 2E_b. \tag{12}$$

By chosing a large enough energy of the secondary electron E_b one can make the second term in the right-hand side of (12) negligible. The integrated cross-section is then written as

$$\frac{\mathrm{d}\sigma_j}{\mathrm{d}\Omega_a\, \mathrm{d}\Omega_b\, \mathrm{d}E_a} = (2\pi)^4 N\, \frac{k_a k_b}{k_0} \left(\frac{\mathrm{d}\sigma}{\mathrm{d}\Omega}\right)_{\mathrm{Mott}} \rho_j(\boldsymbol{q}). \tag{13}$$

As follows from (11) and (13) the (e, 2e) experiment gives the band-specific momentum densities $\rho_j(\epsilon, \boldsymbol{q})$ or $\rho_j(q)$. This is in contrast with the Compton scattering which allows only for obtaining the sum over all occupied bands.

It is of interest to investigate momentum densities in a certain high-symmetry direction in the momentum space, $\boldsymbol{q} = q\hat{\boldsymbol{e}}$, as functions of scalar q. In this case the SMD $\rho_j(\epsilon, q\hat{\boldsymbol{e}})$ becomes a function of only two variables, ϵ and q, and can be presented conveniently as a set of momentum profiles at various energies or energy profiles at various momenta. The EMD $\rho_j(q\hat{\boldsymbol{e}})$ becomes a function of one scalar variable q and can be plotted alongside with the energy bands when the extended zone scheme is used.

Another point of interest is the spherically averaged SMD which can be obtained by integration over the irreducible wedge of the BZ. For the FCC structure:

$$\rho_j(\epsilon, q) = (4\pi)^{-1} \int \mathrm{d}\Omega_q\; \rho_j(\epsilon, \boldsymbol{q}) = \frac{4}{\pi} \int_0^1 \mathrm{d} \sin\vartheta_q \int_0^{\pi/4} \mathrm{d}\varphi_q\; \rho_j(\epsilon, \boldsymbol{q}). \tag{14}$$

This averaging corresponds to the (e, 2e) reaction on a polycrystalline target.

Numerically the spherical integration of (14) is performed on a regular grid of the polar and azimuthal angles ϑ_q and φ_q. This defines a finite mesh of $\boldsymbol{q}$-values, $\boldsymbol{q}_i = (q, \vartheta_i, \varphi_i)$. The SMD is then calculated as a sum of the EMD $\rho_j(\boldsymbol{q}_i)$ weighted with a Gaussian which is centred at the appropriate one-electron energy:

$$\rho_j(\epsilon, q) = A \sum_i \rho_j(\boldsymbol{q}_i)\, \Gamma\left[\frac{\epsilon - E_j(\boldsymbol{q}_i)}{\delta\epsilon}\right]. \tag{15}$$

Here we replace the δ-function in the expression of the SMD (4) by a Gaussian to simulate a finite energy resolution in the experiment, $\delta\epsilon = (8 \ln 2)^{-1/2}$ FWHM, A is a normalization constant. It is seen from (15) that the number of points in the q-mesh required to reproduce a smooth energy profile by overlapping Gaussians depends on $\delta\epsilon$. We found that for all materials considered the 16×16 mesh in polar and azimuthal angles is sufficient to simulate an energy resolution of 1.0 eV which is a realistic value for modern solid-state (e, 2e) techniques (Storer *et al* 1994).

After integration over-energy of the SMD $\rho_j(\epsilon, q)$ of (15) we get a spherically averaged EMD:

$$\rho_j(q) = \int \mathrm{d}\epsilon\, \rho_j(\epsilon, q) \tag{16}$$

which is a function of the scalar q similar to the directional EMD $\rho_j(q\hat{e})$. The spherically averaged EMD obeys an obvious sum rule following from (5):

$$2\sum_j 4\pi \int q^2 \, dq \; \rho_j(q) = N_e. \tag{17}$$

Table 2. Critical-point energies in diamond and silicon (in eV) respect to the valence band maximum at Γ_{25}.

Γ_1	X_1	X_4	L_2	L_1	L_3	Method	Reference
Diamond							
−21.32	−12.60	−6.19	−15.44	−13.36	−2.80	LMTO	Present
−21.28	−12.59	−6.18	−15.43	−13.35	−2.8	LMTO	Glötzel *et al* (1980)
−21.03	−12.43	−6.27	−15.29	−13.09	−2.82	LCAO	Chelikowsky and Louie (1984)
−23.0			−17.3	−14.4		GWA	Hybertsen and Louie (1986b)
−22.88	−13.80	−6.69	−16.95	−14.47	−2.98	GWA	Rohlfing *et al* (1993b)
−21(1)			−15.2(3)	−12.8(3)		Exp.	Himpsel *et al* (1980)
Silicon							
−11.93	−7.75	−2.72	−9.54	−6.94	−1.13	LMTO	Present
−11.87	−7.75	−2.72	−9.53	−6.93	−1.05	LMTO	Glötzel *et al* (1980)
−12.36	−7.69	−2.86	−9.55	−6.96	−1.23	EPM	Chelikowsky and Hohen (1976)
−12.04		−2.99	−9.79	−7.18	−1.27	GWA	Hybertsen and Louie (1986b)
−12.04	−8.01	−2.98	−9.77	−7.21	−1.24	GWA	Rohlfing *et al* (1993b)
−12.5(6)		−2.9	−9.3(4)	−6.8(2)	−1.2(2)	Exp.	Masovic *et al* (1983)
−12.4(6)		−2.5(3)		−6.4(4)		Exp.	Masovic *et al* (1983)
					−1.5	Exp.	Himpsel *et al* (1981)
					−1.6	Exp.	Uhrberg *et al* (1985)
		−3.4				Exp.	Wachs *et al* (1985)

4. Results and discussion

4.1. Band structure

The valence band structure of the diamond-like semiconductors has been studied extensively in recent years both by theory and experiment. A vast amount of data are available in the literature. It is not the aim of the present paper to improve on the accuracy of the calculated band structure or achieve better agreement with experiment. The only reason for which we present here our band-structure results is to test the implementation of the LMTO method and the choice of the atomic sphere parameters. This is done by comparing valence band energies at several high-symmetry points obtained in the present calculation with the most recent and presumably most accurate theoretical and experimental data available to date. Besides the LMTO method the following methods were used in previous calculations: the empirical pseudopotential method (EPM), linear combination of atomic orbitals (LCAO), the GW approximation (GWA) which is an expansion of the self-energy operator in terms of the dynamically screened Coulomb interaction (W) and the dressed Green's function (G). All these data are collected in table 2 (diamond and silicon) and table 3 (germanium and tin). The latter crystals exhibit stronger spin–orbit interaction resulting in band splitting. We do not include explicitly spin–orbit interaction in our calculation and compare our data with the nearest symmetry point corresponding to non-zero splitting.

One can see from the tables that our results are very close to the previous LMTO calculation of Glötzel *et al* (1980). In general our data are fairly close to the experimental

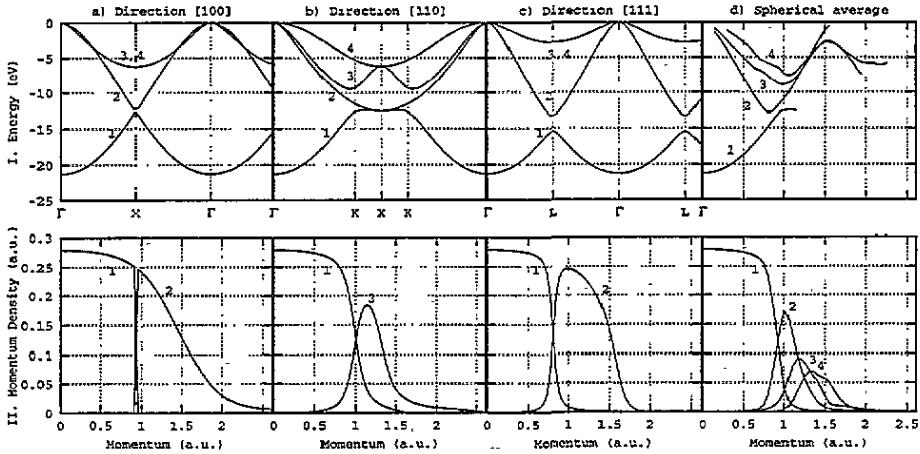

Figure 1. Diamond. Energy bands $E_j(q-G)$ (I) and electron momentum densities $\rho_j(q)$ (II), $q = q\hat{e}$ in the [100], [110] and [111] directions ((a)–(c)) and as the spherical average (d).

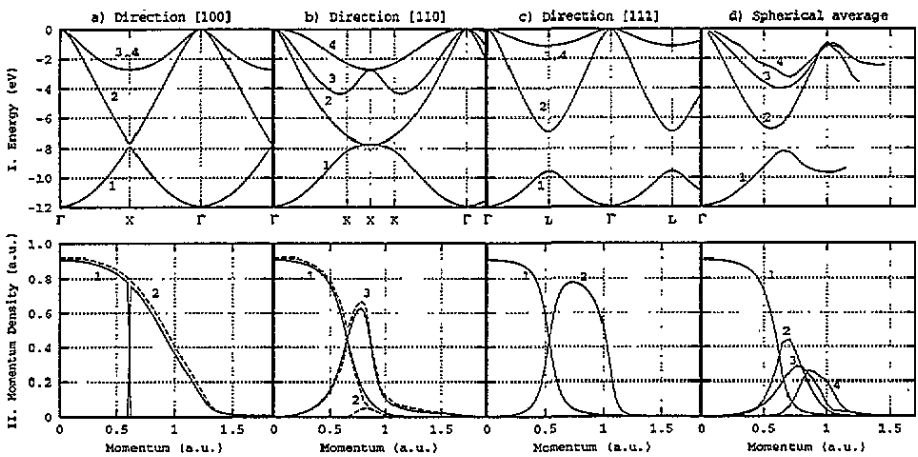

Figure 2. Silicon. As figure 1. Broken lines in the [100] and [110] MD plots show the local pseudopotential calculation of (Schülke 1974).

results with deviations generally not exceeding the difference between experimental results from various groups.

We also plot energy bands $E_j(q)$, $q = q\hat{e}$, as continuous functions of momentum value q in directions [100], [110] and [111] for diamond, silicon, germanium and grey tin as shown in panels I-a to I-c (top row) of figures 1–4, respectively. Where the momentum value q extends outside the first BZ the band structure is obtained by translation of a reciprocal-lattice vector to bring q back to the first zone as indicated in (4). This allows for continuous identification of each band by the band index 1 to 4 and relates the energy of the bound electron with the momentum value q as measured in the (e, 2e) experiment (equation (10)).

In the same figures 1–4 we also show the spherically averaged band energies as functions of momentum (panels I-d, top row). The detailed procedure for obtaining these bands is described in the next section.

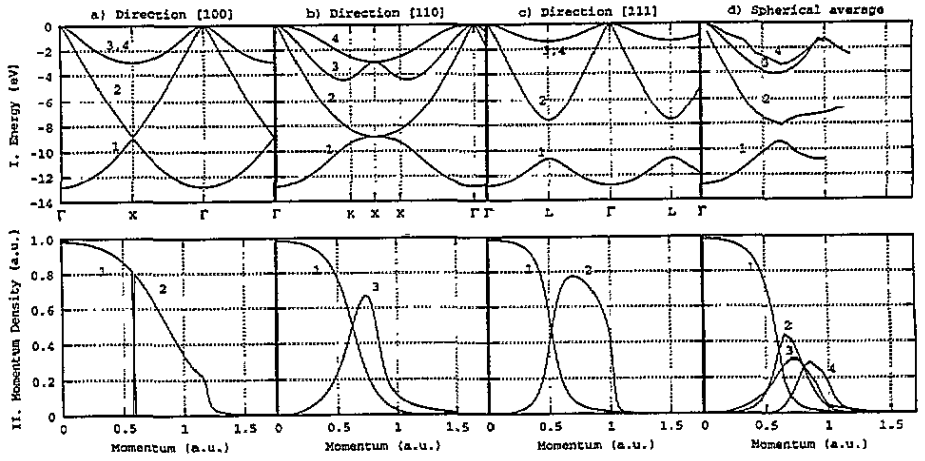

Figure 3. Germanium. As figure 1.

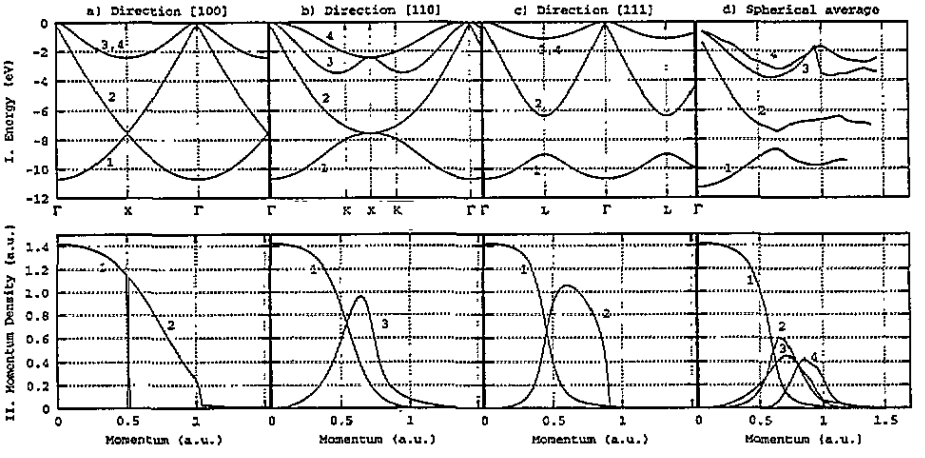

Figure 4. Grey tin. As figure 1.

4.2. Momentum density

We plot the EMD $\rho_j(q)$, $q = q\hat{e}$, as functions of momentum q in directions [100], [110] and [111] for diamond, silicon, germanium and grey tin in panels II-a to II-c (bottom row) of figures (1–4), respectively. The same momentum scale and band labels are used in the energy band and momentum density plots in each direction. These two plot types allow us to reconstruct easily the SMD as a function of momentum and energy in each direction. Indeed, as follows from (4), the SMD $\rho_j(\epsilon, q)$ can be viewed as the energy-independent EMD $\rho_j(q)$ governed in the energy scale by the band energy $E_j(q - G)$.

In direction [100] the SMD follows a free-electron-like parabola along band 1. It switches instantly to band 2 at the first BZ boundary and follows band 2 through the second and third BZ where the absolute value of the SMD drops to zero. In direction [110] the SMD goes through the first BZ as a free-electron-like band 1. Near the zone boundary band 3 starts to contribute and the SMD switches continuously from band 1 to band 3. It follows band 3 all the way to the third BZ where it vanishes gradually. The same pattern can be observed in direction [111] where the SMD goes along band 1 and then band 2. One can also notice

Table 3. Critical-point energies in germanium and grey tin (in eV) respect to the valence band maximum at Γ_8.

Γ_6	X_5	X_5	L_6	L_6	$L_{4,5}$	Method	Reference
Germanium							
−12.82	−8.87	−2.98	−10.65	−7.63	−1.37	LMTO	Present
−12.50	−8.57	−3.01	−10.33	−7.46	−1.37	LMTO	Glötzel *et al* (1980)
−12.66	−8.65	−3.29	−10.39	−7.61	−1.43	EPM	Chelikowsky and Hohen (1976)
−12.86	−9.13	−3.22	−10.89	−7.82	−1.43	GWA	Hybertsen and Louie (1986b)
−12.84	−9.06	−3.16	−10.82	−7.81	−1.47	GWA	
−12.6		−3.2(2)	−10.6(5)	−7.7(2)	−1.4(3)	Exp.	Grobman *et al* (1975)
−13	−9	−3.5				Exp.	Hsieh *et al* (1984)
−12.9(2)	−9.3(2)	−3.5(2)				Exp.	Wachs *et al* (1985)
Grey tin							
−10.71	−7.57	−2.45	−9.02	−6.40	−1.15	LMTO	Present
−10.43	−7.46	−2.56	−8.88	−6.30	−1.04	LMTO	Brudevoll *et al* (1993)
−11.34	−7.88	−2.75	−9.44	−6.60	−1.20	EMP	Chelikowsky and Hohen (1976)
−11.2(2)	−7.9(1)	−2.8(1)				Exp.	Middelmann *et al*

that some bands do not contribute to the SMD along these high-symmetry directions. These include bands 3, 4 in the [100] and [111] directions, and bands 2, 4 in the [110] direction.

This behaviour of the SMD in high-symmetry directions can be understood in terms of the irreducible representation of the point group of the crystal momentum vector (Harthoorn and Mijnarends 1978) and is typical for all diamond structure crystals. A contribution from any particular band to the EMD will be non-zero only if the operator $\exp(-i\boldsymbol{q}\cdot\boldsymbol{r})$ in (4) contains a part transforming to the same representation as a basis function $\psi_{j\boldsymbol{k}}(\boldsymbol{r})$. In the first BZ where $\boldsymbol{p}=\boldsymbol{k}$ only bands belonging to the totally symmetric representations (i.e. Δ_1, Σ_1, Λ_1) contribute to the EMD. These are band 1 in [100] direction, bands 1 and 3 in [110] direction and bands 1 and 2 in [111] direction. For cubic structures with one atom per elementary cell, this selection rules also hold outside the first BZ. However, for two-atom diamond structure the Fourier transform (9) acquires an additional multiplier $\exp(-i\boldsymbol{G}\cdot\boldsymbol{r}_s)$. For this reason occupation switches from band 1 to band 2 in direction [100]. For other directions the same bands continue to be occupied outside the first BZ. For general momenta lying outside any symmetry direction there is only one representation, the totally symmetric one, and therefore all four bands contribute to the SMD. This is clearly seen when the spherical average of the EMD is taken.

In contrast with energy band calculations very little work has been previously done on band-resolved EMD in diamond structure semiconductors. On the theoretical side, we found only one publication of (Schülke 1974) which contains the EMD of silicon in [100] and [110] directions. The local pseudopotential method was used in this calculation. We plot these data along with our results in figure 5, panels II-a and II-b. There is a good agreement between the two calculations except a discontinuity in the EMD of Schülke in the direction [110]. Our data do not have this discontinuity, which is only typical for crossing bands as in the case of [100] direction. There is also a small contribution from band 2 in the second BZ in the [110] EMD of Schülke which is not allowed from symmetry considerations and is absent in our calculation.

Experimentally, the (e, 2e) reaction allows direct determination of the EMD. However, no experiment has been done so far on an oriented crystalline target. The measurements reported to date (Vos *et al* 1994, 1995b, a, Cai *et al* 1995b, a, Storer *et al* 1995) have been performed on polycrystalline or amorphous thin films. These data can be analysed in

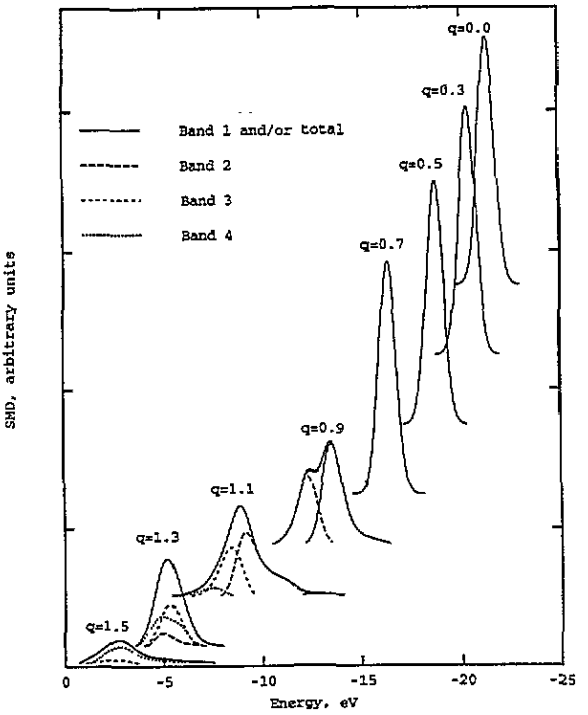

Figure 5. The spherically averaged spectral momentum density $\rho_j(\epsilon, q)$ of (14) in diamond as a function of energy at constant momenta. Energy is relative to the valence band maximum.

terms of the spherically averaged SMD or EMD. Here we present our calculations of these densities which we produce with the numerical procedure described in section 3. First we generate the SMD $\rho_j(\epsilon, q)$ of (14). As an example we show the spherically averaged SMD for diamond as a series of energy profiles at various momenta in figure 5. Different plots are shifted vertically to accommodate several profiles in the same figure. Different line styles denote partial contributions from bands 1 to 4 to each energy profile. We integrate these partial contributions over energy according to (16) to get the spherically averaged EMD $\rho_j(q)$ for each band as a function of momentum value q which we plot in panel II-d of figures 1–4. By tracing the peak position of the partial band contribution to the energy profiles we obtain the spherically averaged band dispersions which we plot in panel I-d of figures 1–4.

The pattern of the spherically averaged bands is changing significantly from diamond to tin. When they are viewed together with the EMD, the spherically averaged bands in diamond follow almost continuously a free-electron-like parabola whereas in silicon there appears a gap between bands 1 and 2. In germanium and tin there is an additional gap between bands 2 and 3 which breaks down the free-electron-like picture that is seen in diamond. In all cases the combined density drops to zero at a position roughly corresponding to the centre of the second BZ where we can no longer trace unambiguously peak positions of partial band contributions.

This tendency can also be seen in grey-scale plots of figure 6 where the SMD $\rho_j(\epsilon, q)$ is presented in linear grey scale as a function of energy and momentum for the all the materials considered. Here lighter shading corresponds to greater intensity. This type of plot gives the most complete picture of the spherically averaged SMD. Clearly the SMD for

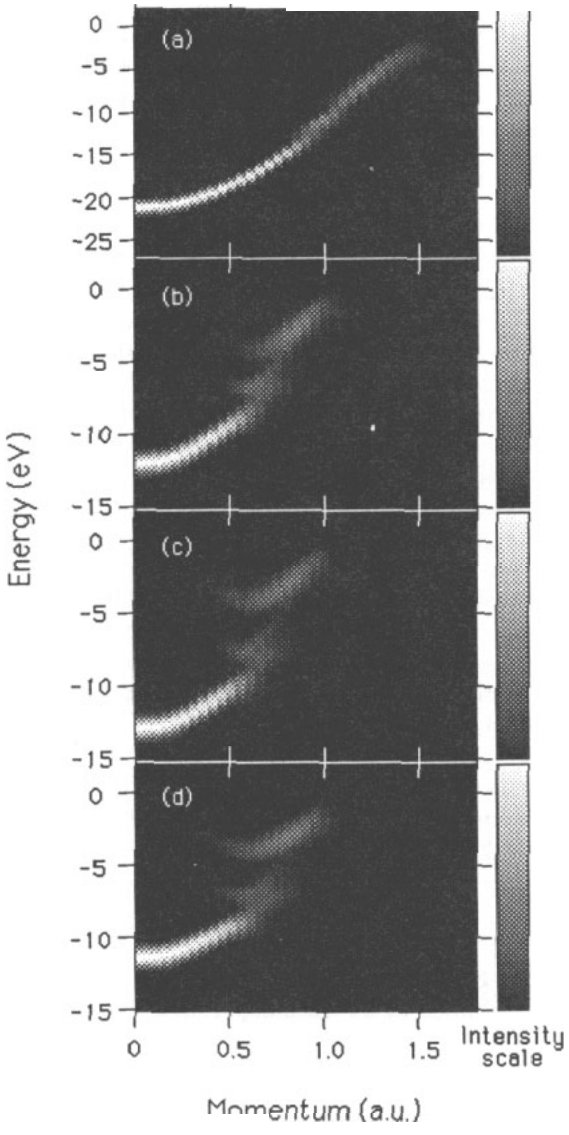

Figure 6. A linear grey-scale plot of the SMD $\rho_j(\epsilon, q)$ as a function of energy and momentum. (a) Diamond. (b) Silicon. (c) Germanium. (d) Grey tin. Lighter shading represents greater intensity.

diamond resembles a free-electron-like parabola. For silicon, germanium and tin, although the gap between bands 1 and 2 is still visible, the two bands appear to be touching each other. The band gap between bands 2 and 3 is clearly visible and becomes bigger going from silicon to tin.

When presented in the same form, as a linear grey-scale plot, experimental data on diamond (Storer *et al* 1995), silicon (Vos *et al* 1995a) and germanium (Cai *et al* 1995a) resemble very strongly our theoretical calculations. The dispersion of the main feature is in excellent agreement with our calculations. However, except for in germanium, no interband

gaps are seen in the experiment. This might well be because of a significantly poorer energy resolution in the experiment (about 2 eV rather then 1 eV which we used in our convolution procedure). Also, the materials studied experimentally were amorphous and the question has to be answered of to what extent these results can be compared with our calculations for randomly oriented crystals.

5. Conclusion

The valence band electron energy and momentum distributions in the form of band dispersion curves and band-specific electron momentum densities have been calculated for diamond, silicon, germanium and grey tin along [100], [110] and [111] directions using the LMTO method with four atomic spheres per elementary cell. While the valence-band-structure results are essentially the same as previously calculated, which lends assurance to the correct implementation of the LMTO method, the calculated SMD are the first of this type. The spherically averaged SMD have also been calculated by angular integration of the Gaussian-weighted EMD over repeating part of the FCC BZ. The spherically averaged band dispersion resembles a free-electron-like parabola for diamond whereas in the case of the other materials band gaps appear between the averaged bands.

These data can be used for interpreting results of the (e, 2e) experiment in the form of the fully differential cross-section or energy-integrated triply differential cross-section on both oriented or disordered or amorphous targets. When compared with recent experimental results on amorphous diamond, silicon and germanium, the calculated spherically averaged SMD shows very close resemblance with the experiment. However, better energy resolution is desirable to show more clearly the interband gaps.

The full testing of the electron momentum distributions in the materials studied can be achieved when the experiments on oriented crystalline targets become possible. Such experiments will have enormous potential for providing a thorough understanding of the electronic structure of these technologically important solids.

Acknowledgments

We wish to thank Professors I E McCarthy and Professors E Weigold for stimulating discussions. This work was supported by an Australian Research Council grant.

References

Allen L J, McCarthy I E, Maslen V W and Rossouw C J 1990 *Aust. J. Phys* **43** 453
Bachelet G B and Christensen N E 1985 *Phys. Rev.* B **31** 879
Bassani F, Fumi F and Tosi M P (ed) 1985 *Highlights of Condensed-Matter Theory* (Amsterdam: North-Holland)
Brudevoll T, Citrin D S, Cardona M and Christensen N E 1993 *Phys. Rev.* B **48** 8629
Cai Y Q, Storer P, Kheifets A S, McCarthy I E and Weigold E 1995a *Surf. Sci.* at press
Cai Y Q, Vos M, Storer P, Kheifets A S, McCarthy I E and Weigold E 1995b *Phys. Rev.* B at press
Chelikowsky J R and Cohen L 1976 *Phys. Rev.* B **14** 4450
Chelikowsky J R and Louie S G 1984 *Phys. Rev.* B **29** 3470
Cohen M L and Chelikowsky J R 1988 *Electronic Structure and Optical Properties of Semiconductors* (Berlin: Springer)
Cooper M J 1985 *Rep. Prog. Phys.* **48** 415
Glötzel D, Segall R and Andersen O K 1980 *Solid State Commun.* **36** 403
Grobman W D, Eastman D E and Freeouf J L 1975 *Phys. Rev.* B **12** 4405
Harthoorn R and Mijnarends P E 1978 *J. Phys. F: Met. Phys.* **8** 1147
Himpsel F J, Heimann P and Eastman D E 1981 *Phys. Rev.* B **24** 2003

Himpsel F J, van der Veen J F and Eastman D E 1980 *Phys. Rev.* B **22** 1967
Hohenberg P and Kohn W 1964 *Phys. Rev.* **136** B864
Hsieh T C, Miller T and Chiang T C 1984 *Phys. Rev.* B **30** 7005
Hybertsen M S and Louie S G 1986a *Phys. Rev.* B **34** 5390
——1986b *Phys. Rev.* B **34** 5390
Jain P C, Singru R M and Gopinathan K P ed 1985 *Positron Annihilation* (Singapore: World Scientific)
Kohn W and Sham L J 1965 *Phys. Rev.* **140** A1133
Leckey R C G and Riley J D 1992 *CRC Crit. Rev. Solid State Sci. Technol.* **17** 307
Lundqvist S and March N H (ed) 1983 *Theory of the Inhomogeneous Electron Gas* (New York: Plenum)
Masovic D R, Vukajlovic F R and Zekovic S 1983 *J. Phys. C: Solid State Phys.* **16** 6731
McCarthy I E and Weigold E 1988 *Rep. Prog. Phys.* **51** 299
——1991 *Rep. Prog. Phys.* **54** 789
Middelmann H U, Sorba L, Hinkel V and Horn K 1987 *Phys. Rev.* B **35** 718
Ortega J E and Himpsel F J 1993 *Phys. Rev.* B **47** 2130
Persiantseva N M, Krasil'nikova N A and Neudachin V G 1991 *Sov. Phys.– JETP* **49** 530
Rohlfing M, Krüger P and Pollmann J 1993a *Phys. Rev.* B **48** 17791
——1993b *Phys. Rev.* B **48** 17791
Schülke W 1974 *Phys. Status Solidi* b **62** 453
Skriver H L 1984 *The LMTO Method* (Berlin: Springer)
Storer P, Caprari R S, Clark S A, Vos M and Weigold E 1994 *Rev. Sci. Instrum.* **65** 2214
Storer P, Vos M, Cai Y Q, Canney S, Weigold E and Kheifets A S 1995 *Appl. Phys. Lett* at press
Uhrberg R I G, Hansson G V, Karlsson U O, Nicholls J M, Persson E S, Flodstrom S A, Engelhardt R and Koch E E 1985 *Phys. Rev.* B **31** 3795
Vos M, Storer P, Cai Y Q, Kheifets A S, McCarthy I E and Weigold E 1995a *J. Phys.: Condens. Matter* at press
Vos M, Storer P, Cai Y Q, McCarthy I E and Weigold E 1995b *Phys. Rev.* B at press
Vos M, Storer P, Canney S, Kheifets A S, McCarthy I E and Weigold E 1994 *Phys. Rev.* B **50** 8
Wachs A L, Miller T, Hsieh T C, Shapiro A P and Chiang T C 1985 *Phys. Rev.* B **32** 2326